Author:	Indiketiya, Samanthi; Jegatheesan, Piratheepan; Rajeev, Pathmanathan
Title:	Evaluation of defective sewer pipe induced internal erosion and associated ground deformation using laboratory model test
Year:	2017
Journal:	Canadian Geotechnical Journal
URL:	http://hdl.handle.net/1959.3/434967
Copyright:	Copyright © 2017 NRC Research Press. The author's accepted manuscript is reproduced here in accordance with the copyright policy of the publisher. The published version is available at https://doi.org/10.1139/cgj-2016-0558.

Canadian Geotechnical Journal
Revue canadienne de géotechnique

Evaluation of Defective Sewer Pipe Induced Internal Erosion and Associated Ground Deformation Using Laboratory Model Test

Journal:	*Canadian Geotechnical Journal*
Manuscript ID	cgj-2016-0558.R1
Manuscript Type:	Article
Date Submitted by the Author:	n/a
Complete List of Authors:	Indiketiya, Samanthi; Swinburne University of Technology, Civil and Construction Engineering; Jegatheesan, Piratheepan; Swinburne University of Technology, Rajeev, Pathmanathan; Swinburne University of Technology, Civil and Construction Engineering
Keyword:	PIV, Sinkholes, Ground subsidence, Physical-model, Pipe leakage

Evaluation of Defective Sewer Pipe Induced Internal Erosion and Associated Ground Deformation Using Laboratory Model Test

Samanthi Indiketiya[1], Piratheepan Jegatheesan[2] & Pathmanathan Rajeev[3]

[1] Ph.D. candidate, Swinburne University of Technology, Melbourne, Vic 3122, Australia, sindiketiyahewage@swin.edu.au

[2] Senior Lecturer, Swinburne University of Technology, Melbourne, Vic 3122, Australia, pjegatheesan@swin.edu.au

[3] Senior Lecturer, Swinburne University of Technology, Melbourne, Vic 3122, Australia, prajeev@swin.edu.au

Corresponding Author

Name: Piratheepan Jegatheesan

Address : Swinburne University of Technology, Melbourne, Vic 3122, Australia

Telephone : +61 392145859

E-mail : pjegatheesan@swin.edu.au

Abstract

Sinkholes induced by long-term internal erosion around defective sewer pipes have been widely reported. There is a need for an efficient method to understand the influence of pipe defects on internal erosion and ground settlement. This paper presents an approach to the investigation of erosion-induced ground settlement and the susceptibility of pipe bedding materials to internal erosion. A new and efficient erosion test apparatus is introduced, and aided by controlling most of the key influencing parameters. The corresponding ground displacement is tracked by image correlation based on particle image velocimetry (PIV). The basic parameters investigated are: (1) the process of cavity initiation and evolution, (2) the rate of soil loss, (3) the gradation of eroded soil, (4) the corresponding ground displacement. The results indicate that particles less than 0.3 mm are highly vulnerable to erosion through 5 mm openings of embedment material with a maximum particle size of 4.75 mm. The proposed method is beneficial, since it allows measurement of the deformation at any time and at any location throughout the test and facilitates checking the resistance to erosion of pipe embedment materials.

Keywords: PIV, Sinkholes, Ground subsidence, Physical model, Pipe leakage, Sewer pipe

Introduction

Over the last few decades, the frequency of sinkhole formation due to internal erosion around defective sewer pipes has increased (Weil 1995; Tohda and Hachiya 2005; Guo et al. 2013). Sewer pipes deteriorate with time, resulting in cracks, fractures and openings that allow soil in the vicinity to migrate into the pipe during ground water infiltration and instantaneous sewer exfiltration processes (Bertrand-Krajewski et al. 2006; Cardoso et al. 2006; Meguid and Dang 2009; Karpf et al. 2011). The continuation of this process over a prolonged period forms a cavity around the defect with an associated low-strength zone, which propagates towards the ground surface with groundwater fluctuation, finally causing a sinkhole (Zheng 2007; Balkaya et al. 2012; Guo et al. 2013). Sinkholes represent a substantial economic loss, as they can initiate a series of catastrophic events including interruption to buried service lines (water, cable, electric, gasoline, and telephone), disruption to traffic, contamination of nearby natural water bodies by sewer overflow, sewer overflow in residences upstream, damage to highway profiles and sometimes human fatalities (Galve et al. 2012). Furthermore, soil erosion from the vicinity of the pipe causes a loss of support from the surrounding soil to the pipe, which may completely lose its structural integrity and break (Abraham and Wirahadikusumah 1999; Moore 2008; Balkaya et al. 2012). In addition, soil and ground water flow into sewer pipes through defects increases the operating cost of wastewater treatment and pumping stations, especially in rainy seasons. For example, in Australia, ground water infiltration into waste water systems is 12% of the total collected flow (Institute of Public Works Engineers Australia 2010).

Kuwano et al. (2006) reported that pipe defects significantly increased in pipes older than 25 years and, importantly, many cities worldwide have a large percentage of pipes that are 25 years or older. For example, in many German systems over 54% of the pipes are older than 25 years and 24% are older than 50 years (Burn et al. 1999). In Australia, the systems are generally newer, and a typical system has only 47% of pipes that exceed 25 years of age and 13% older than 50 years (Burn et al. 1999). Therefore, pipe defects can be expected worldwide which can lead to life-threatening sinkholes, and it is very useful to be aware of the danger and to find suitable mitigation measures.

This paper introduces a new experimental methodology utilising particle image velocimetry (PIV) to study the internal erosion process and void formation in the vicinity of pipe defects. A two-dimensional model ground with an opening at the base is used to represent a defective sewer and the influence of frequent exfiltration and infiltration of water through a pipe defect on sinkhole development was investigated.

Soil Migration through Pipe Defects and Influencing Parameters

Several researchers have studied the mechanism of soil erosion through pipe defects and a number of parameters have been identified as potentially significant. These include the width of the defect in a sewer, the particle size distribution, the plasticity and density of backfilling material, fluctuation of the groundwater table, ground water infiltration and sewer exfiltration through the defect (Rogers 1986; Fenner 1991; Otani et al. 2000; Mukunoki et al. 2006; Mukunoki et al. 2007; Sato and Kuwano 2008; Mukunoki et al. 2009; Renuka and Kuwano 2011; Kuwano et al. 2012; Mukunoki et al. 2012; Guo et al. 2013; Sato and Kuwano 2013; Sato and Kuwano 2015a, b).

Defect size (crack width) is a crucial factor affecting the scale of soil loss (Mukunoki et al. 2012). Specifically, a relationship has been proposed between soil loss and the ratio of B/ D_{85} for fine sand and gravels under one-way flow, where D_{85} is the size of sieve through which 85% by weight of a soil sample will pass and B is the crack width (Rogers 1986). A critical crack width for continuous migration of soil was expressed as $2.5D_{85}$ to $4.5D_{85}$. More recently, Mukunoki et al. (2012) presented the critical crack width (B) for the cyclic behaviour of water inflow and drainage for a similar type of soil as 5.9D_{max}, where D_{max} is the maximum particle size. Both relationships confirm that soil loss is critical when the crack width exceeds the maximum particle size.

Another key factor that controls the rate and volume of soil loss is the internal stability of the soil. This factor has been extensively studied (Istomina 1957; Kenney and Lau 1985; Burenkova 1993; Chang and Zhang 2013). Summarising these findings, Chang and Zhang (2013) revealed that internal stability depends on geometric conditions (i.e., grain size and its distribution, pore size and distribution), hydraulic conditions (i.e., hydraulic gradient, moisture content, flow velocity and flow direction) and mechanical conditions of the ground (i.e., compaction effort and apparent cohesion).

A number of studies have also suggested that a high relative density provides a massive advantage against soil loss and cavity propagation in granular material (Sato and Kuwano 2008; Renuka 2012). However, Rogers (1986) and Benahmed and Bonelli (2012) proposed that the relative density has no significant influence on the erosion resistance of clay material, but a high percentage of clay in the soil and a low moisture content of the soil do enhance erosion resistance.

The extent to which soil migration occurs also depends on the type of bedding used around the pipe. It is well known that if granular material surrounds a pipe, water movement is easier in the bedding and this may wash fines out of the surrounding backfill. As a result most specifications (Water Services Association Australia 2002) indicate that migration of fines into the bedding zone from the backfill must be prevented by surrounding the bedding material with a geotextile. Furthermore, Fenner (1991) investigated the mechanism of soil migration in different types of pipe beddings specified by the British Standards Institution (1987) and recommended class-F bedding (Flatbed) over Class-S bedding (pipe fully surrounded by granular material) based on the soil loss and the ground settlement.

Possible methods of minimizing the occurrence of sinkholes are either: (1) avoid the development of pipe defects (Davies et al. 2001), (2) enhance the internal stability of pipe embedment material against internal erosion (Sato and Kuwano 2008) or (3) detect cavities early by regular geophysical surveys such as ground penetrating radar (GPR) (El-Qady et al. 2005). Of these options, the second is highly effective, since it can be achieved without any additional construction or maintenance cost.

Review of Previous Erosion Apparatuses for Soil Erosion through Pipe Defects

A number of studies have investigated the behaviour of soil flow through defective sewers using experimental procedures (Rogers 1986; Kuwano et al. 2006; Mukunoki et al. 2009; Sato and Kuwano 2010; Guo et al. 2013). The key features and capabilities of these previous experimental set-ups are discussed in this section.

Controlled crack width is necessary for the apparatus since it is important to identify the critical crack size for a particular soil type. Rogers (1986) developed two different test apparatuses (small and large) to determine the rate of soil loss. In the small apparatus, the crack width is gradually increased during infiltration to achieve the onset of soil migration. However, in reality, internal erosion is a chronic phenomenon and crack width changes very slowly. Hence, the findings can be misleading. This issue was then considered in the large apparatus by introducing an actual defective pipe into the model ground. However, conducting experiments with different pipe sizes and crack widths requires changing the pipe in the experimental setup. This is expected to be a difficult process and may cause failure in the setup such as water leakage from wall-pipe interface connections. Mukunoki and colleagues (Mukunoki et al. 2006; Mukunoki et al. 2009; Mukunoki et al. 2012) introduced a cylindrical model tank with various crack widths and orientations, and, using this model, it was revealed that the orientation of the crack is not significant, but rather it is the crack width and the area exposed to the ground that is important for soil loss. Other test approaches have often been based on a single crack width, either rectangular in shape (Mukunoki et al. 2006; Sato and Kuwano 2008; Renuka and Kuwano 2011; Kuwano et al. 2012; Sato and Kuwano 2013) or a circular orifice (Guo et al. 2013).

Sewer depth is also a crucial factor which determines the possibility of pipe defects and the scale of erosion (O'Reilly et al. 1989). The minimum and maximum cover required over sewers are specified by authorities, depending on the type of pipe and the application of ground surface (e.g. United States Department of the Interior 1996; Water Services Association Australia 2002; Drainage Services Department 2013). All of the above-mentioned test methods are capable of controlling the surcharge either by means of compressed air (Mukunoki et al. 2006; Mukunoki et al. 2009; Mukunoki et al. 2012; Ke and Takahashi 2014), water (Rogers 1986; Guo et al. 2013) or by surcharge weights (Sato and Kuwano 2008; Renuka and Kuwano 2011; Sato and Kuwano 2013). While accurate and uniform pressure can be achieved with compressed air using a pressurised air bladder (Brachman et al. 2000, 2001), it is challenging to use pressurised air bladder in a small model tank due to boundary constraints. The problem with a latex bag filled with water is the danger of leakage caused by sudden damage and the difficulty of representing larger values of surcharges.

Controlled seepage is another essential requirement to ensure that the most of the actual ground issues are simulated by the apparatus. Soil loss into defective sewers is possible either by ground water infiltration or sewer exfiltration (cyclic flow), due to temporary variations in the sewer system. Most of the previously-introduced methods have been designed for both monotonic and reversed flow conditions (Rogers 1986; Mukunoki et al. 2006; Mukunoki et al. 2007; Sato and Kuwano 2008; Mukunoki et al. 2009; Renuka and Kuwano 2011; Mukunoki et al. 2012; Sato and Kuwano 2013).

Apart from the flow direction, a controlled flow rate is also essential to maintain a similar hydraulic pressure throughout the test and to accurately predict the volume of the total water flow. Earlier studies used a fixed volume of water inflow per cycle or per test (i.e. head is not constant), whereas later studies used a constant-water-head tank to achieve a constant flow rate throughout the test. One common issue with the constant-water-head tank is the dissolution of air which flows into the model tank through the main supply when the full flow is not maintained (Kenney and Lau 1985). The same can be observed at the flow outlet which disturbs the surrounding ground close to the entrance. Therefore, full flow in both the main feeding pipe and the outflow pipe is advised to minimise disturbance by aeration. This can be further reduced by introducing a porous plate to the base of the tank, which reduces the turbulence caused by inflow or outflow.

Most of the apparatuses described previously were designed to collect the eroded mass by flat end, box type devices connected to the pipe defect. Nevertheless, eroded soil particles can easily clog at the flat base or around the surface of tube-shaped devices, leading to incorrect measurement of soil loss corresponding to each cycle. To overcome this issue, Indraratna et al. (1996) proposed a device with a conical base which increased the accuracy of measurements.

Displacement tracking close to the ground surface is an essential requirement, since it is very useful in understanding the extent of the impact on structures. Installing displacement transducers into the model ground may disturb the soil migration patterns, as the transducers have a reinforcing effect on the soil (Ng et al. 2002). Moreover, it is hard to achieve a deformation profile with a higher resolution, since it requires a greater number of sensors, which makes the disturbance even greater. Therefore, there remains a need for an effective method for non-intrusive displacement tracking around defective sewers.

Based on this review of previous test approaches, the crucial features required for an effective erosion test apparatus can be identified. An effective approach should be able to: (1) control the seepage direction, flow rate, crack width and surcharge, (2) minimise the scale and boundary effects, (3) track the ground deformation close to the defective pipe and the ground surface, (4) measure the eroded soil mass and analyse the particle size distribution, (5) identify the extent of loosening, (6) measure the properties of eroded mass and (7) minimise sidewall leakage. At present, there is no single apparatus that has been designed considering all above features. Therefore, after carefully reviewing the strengths and weaknesses of previous methods, an economic, convenient, repeatable and accurate methodology was designed, as described in the next section.

Proposed Erosion Test Apparatus

This study introduces a new approach to the investigation of the erosion susceptibility of pipe embedment materials and the related ground deformation induced by defective sewers using a laboratory model test that closely simulates field conditions. A number of previous experimental approaches were carefully studied, and the disadvantages of these methods were clearly outlined and a new method was developed to address the primary concerns associated with these approaches.

The new method directly investigates not only the characteristics of internal erosion through various sizes of pipe defects, but also the ground deformation around both the pipe defect and the ground surface at any stage of the process. However, the method is highly applicable for coarse-grained soil. A diagram and a photograph of the model apparatus are shown in Figure 1 and Figure 2 respectively. The apparatus consists of six main parts (Figure 2): a central soil chamber, additional side chambers for excess water to develop uniform boundary conditions, an eroded soil collection unit (Figure 3), a crack width control unit (Figure 4), a surcharge application unit and a constant-flow rate-control unit.

In order to minimise the boundary issues with small-scale tests, the central soil chamber is designed to be 800 mm long, 400 mm high, and 100 mm wide. The sidewalls are fabricated with 12 mm thick clear acrylic plates, which are stiff enough not to deflect laterally and thus at-rest lateral earth pressure is expected to be generated within the soil (Brachman et al. 2000). The front and back wall are permanently glued to other cross walls to avoid unnecessary water leakage, and transparent walls allow observation of the internal erosion and settlement from outside. To assist with the control of subsequent layers during model preparation, horizontal lines are marked on both sides of the wall at 50 mm intervals. In addition, vertical lines at 50 mm intervals are marked to assist image analysis by following a grid of 50 mm x 50 mm on each wall. Two side chambers 60 mm in length, 400 mm in height and 100 mm in width are provided on either side of the soil chamber, which is separated from the main chamber by vertical perforated walls. These perforated walls permit water from the main soil chamber to seep into side chambers without carrying soil particles. Therefore, a more precise simulation of real ground condition is achieved by extending the ground-water table in either direction.

A 100 mm diameter circular shaped interchangeable plate is placed at the base to facilitate the change of crack width by replacing the plate with the required size of crack. The top surface of this interchangeable plate with the opening is then fixed level with the base of the soil chamber and this allows the representation of a pipe defect close to its crown. This crack width control unit and eroded soil collection unit are assembled as a single unit. The maximum diameter of the conical shape eroded soil collection device is exactly harmonized with the interchangeable crack width plate which is placed over it and screwed to the base plate of the tank as a unit (Figure 3). To ensure that no water or fine soil particles leak through this connection, an O-ring is embedded along the circumference of the interface of the soil collection unit. A drainage plug is located at the lower end of the conical device which remains closed during water inflow and is opened when drainage is required.

As explained in the previous section, to simulate the overburden pressure acting on a sewer pipe, it is advised to apply the surcharge by compressed air or water. However, utilising the best available resources, the required additional load is transferred to the ground by means of steel weights placed on a solid, horizontal timber plate placed on the ground surface. Exactly half of the required load is suspended by steel rods connected to the loading plate and the rest is placed over it to reduce the impact on the acrylic walls of the tank. Steel plates are placed symmetrically from the centre of the tank and vertically aligned in order to achieve a uniform load distribution, assuming that the density of the timber plate and steel weights are uniformly distributed. Different sewer depth conditions can be simulated by changing the load.

As a controlled flow rate is essential, a constant-head water tank was used in this study. To assist the proper function of the tank, the diameter of the main water inflow pipe from the water main, the overflow pipe and the constant-head outflow pipe from the tank is selected as 5 mm, 10 mm and 4 mm, respectively. Relatively high stiff, clear pipes are used to ensure that the full flow is maintained in both the main water pipe and the outflow pipe. This also minimises the formation of air bubbles in the constant-head outflow pipe, since it can disturb the full flow condition and these air bubbles can clog around the potential pipe defect affecting the test results. In addition, the water flow rate is calibrated for the specific water head and volume is measured with time.

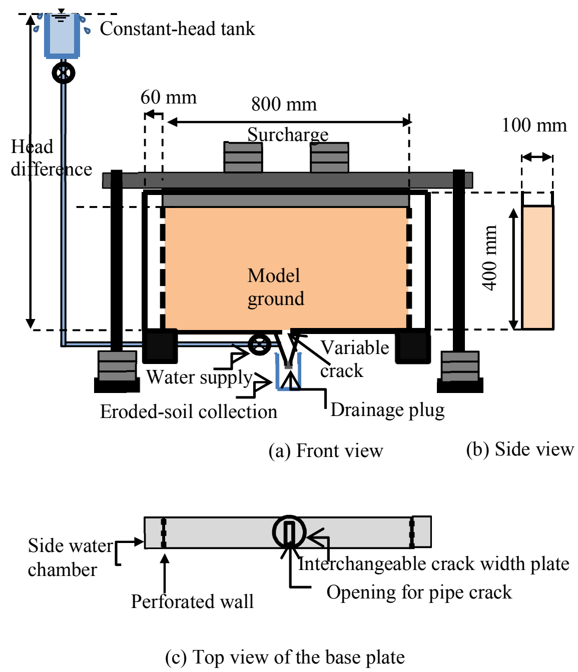

Figure 1: Schematic diagram of the proposed testing apparatus: (a) Front view; (b) Side view; (c) Bottom view

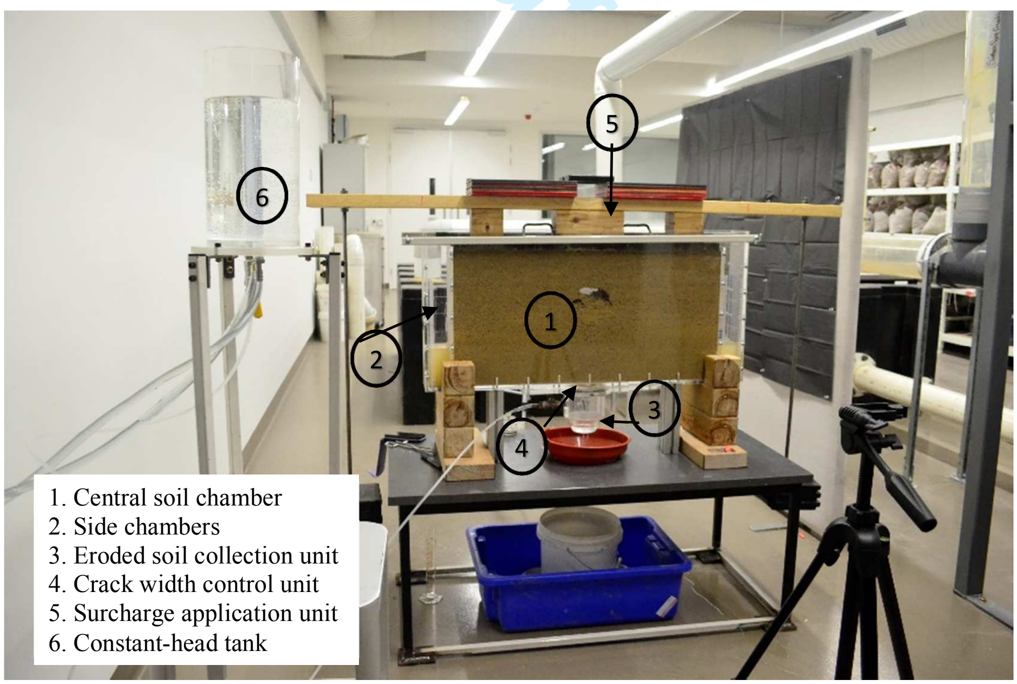

Figure 2: Annotated image of the actual erosion test apparatus

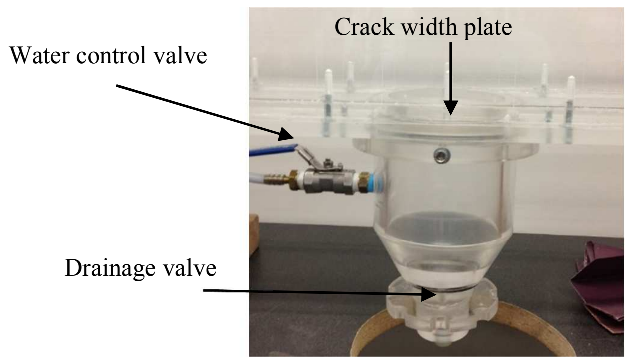

Figure 3: Soil/Water Drainage Unit

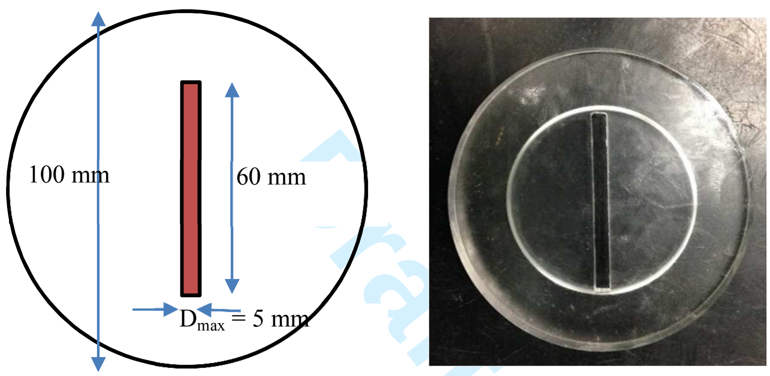

Figure 4: Interchangeable crack width plate

Testing Material

The selection of the sewer embedment material in Australia is based on the Sewerage Code of Australia (Water Services Association Australia 2002), which was developed using Buried Flexible Pipes Standards (Standards Australia 2002). Sand (concrete sand, compaction sand, grade A, grade B), crushed rock (5, 7, 10, 14, 20mm), aggregate (10, 14, 20 mm) and stabilised crushed rock (4-6 % of cement) are widely used bedding materials in Australia (Yarra Valley Water 2013). In this study, a sand known as “Dromana”, which is compatible with approved embedment material type 360 (concrete sand) and type 361 (fine crushed rock) in the Water Services Association Australia (2002) specification, was tested for erosion. The range of the particle size distribution of the Dromana sand and the approved embedment material type 360 and 361 in the Water Services Association guidelines (2002) is shown in Figure 5. Dromana sand consists of clean, coarse-grained, poorly-graded sand particles with angular and sub-angular shapes. It is light yellowish-brown in colour and is derived from brown granite, hence it is also known as granitic sand. Dromana sand can be classified as "SP" according to the Unified Soil Classification System (Corps of Engineers 1953). Other important engineering properties are given in Table 1. The material was prepared for testing by sieving through a 4.75 mm sieve to remove any larger particles and it was then oven-dried for 24 to 48 hours.

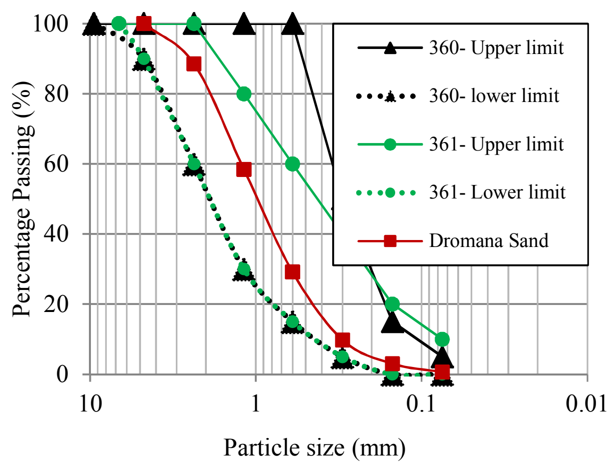

Figure 5: Particle size distribution of Dromana sand

Testing procedure

This study was mainly intended to simulate the reversed flow condition corresponding to water flowing out of the sewer into the soil and then back into the sewer through pipe defects due to temporary fluctuations and surges in sewer flow. As the first step of the procedure, the desired crack width plate was placed level with the bottom plate of the tank, ensuring that the length of the crack was oriented perpendicular to the front and back wall of the tank. Next, the eroded soil collection unit was placed next to the crack width plate, as the crack width plate is eventually supported by this unit. The soil collection and drainage unit were then connected to the base plate of the tank with screws. In order to avoid initial soil loss through the opening during the preparation of the soil box, icing sugar was placed against the opening, which gradually dissolves when the first water cycle flows into the tank. Dromana sand with an optimum moisture content of 11% was then placed in the box and compacted to 70% of relative density. An electric drum mixer was used to mix the soil uniformly without particle segregation. The soil was uniformly placed into the tank by the air-pluviation technique, as described in relative density tests by Standards Australia (1998), and compacted into 50 mm thick layers. The layer height was accurately controlled by horizontal lines marked on the front, back and side walls at intervals of 50 mm and also with the help of the tamper, which can control the maximum drop with respect to the top edge of the tank. The bonding between each layer was achieved by roughening the top surface of each layer of about 3 mm before proceeding to the next layer.

Surcharge loads were then applied on the loading platform that was placed horizontally on the ground surface to simulate 7.5 kPa of vertical earth pressure on top, which developed around 14 kPa at the tank base. After preparing the model ground and applying the required surcharge, the model ground was left for 12 to 15 hours to remove any creep effect. The interface friction between the sidewall and the soil in such experiments is one of the boundary effects which needs to be eliminated or minimised (Tognon et al. 1999; Brachman et al. 2000, 2001). However, in this experiment, the friction effect was considered to be negligible, because the friction between the sand and the Perspex sidewall was deemed to be inconsequential. Liu et al. (2011) reported a friction angle of 14º for coarse sand on Plexiglass. Based on this value, the maximum interface friction generated at the bottom sidewall constitutes approximately 5% of the total overburden pressure, assuming a Poisson's ratio of 0.3 previously demonstrated for sand backfill in a laboratory model test (Brachman et al. 2001). The presence of water in this experiment probably reduced the interface friction well below 5%, as for most of the time the soil was saturated during the infiltration and exfiltration cyclic process. In addition, side wall friction has been considered insignificant in similar laboratory model tests in previous studies (Tsutsumi et al. 2010; Guo et al. 2013; Sato and Kuwano 2015a).

For the present study, the experimental setup simulated a ground with a defective pipe containing a 5 mm wide, 60 mm long crack in the crown. Water passed into the model as a reversed flow pattern where the water was moved back and forth through the defect causing internal erosion. The initial rate of water inflow was maintained at 11 ml/s and the volume of water for each cycle was controlled by time. Although a constant head tank was used, the flow rate may have varied slightly throughout the test since the overall head difference is affected when the water level rises through the soil tank. The duration corresponding to each drainage cycle is given in Table 2. Water flow duration was kept constant for three consecutive cycles and then increased by 30 s. When the appropriate volume of water had passed into the model tank, the drainage valve was closed and the model was left for 2 minutes to stabilize the water level followed by drainage. To avoid accelerated soil loss induced by suction in the drainage unit, pressure close to the crack was slowly released by a small valve before proceeding to complete drainage through the main plug. Subsequently, eroded soil and drained water in each cycle were collected in separate beakers and sieve analysis for each cycle was performed separately after the soil was dried in the oven.

Particle Image Velocimetry (PIV)

Image acquisition and correlation by PIV

The ground displacement corresponding to each drainage cycle was evaluated using image correlation. Specifically, two digital single-lens reflex cameras (DSLR) were arranged either side of the tank at a distance of 1500 mm from the tank, as shown in Figure 6. Setting the camera in close proximity to the object eventually causes perspective distortion in still images (Thielicke 2014). Therefore, a maximum possible distance of 1500 mm was chosen. Nikon D5100 and Nikon D5300 DSLR cameras were used in this study and both cameras included 23.6 x 15.6 mm, complementary metal–oxide–semiconductor (CMOS) sensors and an image resolution of 3696 x 2448 pixels was selected. The cameras and lenses were operated in manual mode to avoid relative movement between the lens and the object which can be expected in automatic mode while autofocussing. Images were acquired at an interval of 1 s using the interval timer option. In addition, two black screens were placed behind each camera to avoid reflection of surrounding objects on Perspex walls that could have triggered noises during image analysis.

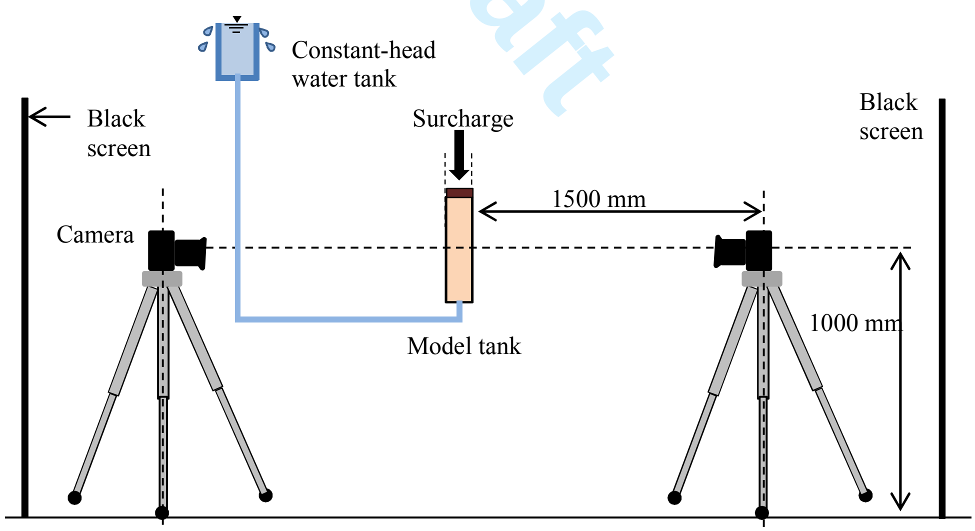

Figure 6: Arrangement of the testing equipment

The obtained images were analysed using PIVlab (Thielicke and Stamhuis 2014), a graphical user interface (GUI)-based open-source tool in MATLAB (The Mathworks Inc 2014). Images were acquired in JPEG format and two sequential frames are defined as a pair. The ground displacement corresponding to each drainage cycle was evaluated in the vicinity of the pipe crack and also close to the top surface of the model ground. The correlation was assessed for each drainage cycle by considering an image pair. The first image was before water infiltration into the model ground and the second was after complete drainage of the same cycle. The horizontal and vertical velocity (u, v) corresponding to each test patch were calculated using PIVlab, which also allows the mean velocity of a user-defined area of the image to be obtained. Using this tool, the mean velocity corresponding to each 50 mm x 50 mm grid on the model wall was obtained and hence, a displacement of each 50 mm thick horizontal layer was evaluated by multiplying each layer by the time gap between images. Finally, the cumulative displacement was obtained, cross-checked and the method was validated by determining the correlation between the first image of the first water cycle and the last image of the 19th cycle.

Validation of PIV

The reliability of displacements measured by the PIV technique was evaluated using a series of experiments by shifting the soil tank with a known displacement. The same tank filled with soil under similar conditions (soil type, moisture content, density, etc.) was vertically displaced at several small translation steps of 0.1 mm, 0.2 mm, 0. 5 mm and 1 mm, using a hydraulic jack. The true displacement of the tank was considered as the average of three linear variable differential transformers (LVDTs) mounted on the tank top, symmetrically at both corners and the centre. Since there is no relative movement between the tank and the soil, the displacement evaluated by PIV can be considered as the soil displacement. Therefore, comparison of the true and evaluated displacement was used to assess the accuracy and precision of the proposed PIV method.

The image-space consisted of 3696 x 2448 pixels which correspond to 1.108 x 0.734 m in object-space. Each pixel represented 0.0003 m in object-space. An interrogation area of 128 x 128 grids was used with a step width of 64 x 64 for image correlation. Accordingly, each image had 13, 294 data points and the vector distribution of every 5th vector is given in Figure 7. For this paper, the accuracy and precision for a 1 mm step of movement are presented. When the true displacement of the tank is 1 mm, the PIV-based evaluated displacements for 13,294 data points were evaluated and the normalised distribution is given in Figure 8.

The magnitude of the total error exists in two components as bias (ε_{bias}) and random (ε_{rms}) error (Raffel et al. 2007) as given in Equation 1 and 2. The bias error defines the trueness of the estimated displacement and the random error determines the precision of the estimated displacement (Thielicke 2014). For this case, the bias error of 0.000149 mm and random error of 0.0297 mm is determined with the mean measurement for a total of 13 294 data points of 1.0068 mm. Therefore, considering the requirement of the suggested method, the accuracy of PIV analysis is sufficient and shows good agreement with the true displacement.

$$\varepsilon_{bias} = \frac{1}{n} \sum_{i=1}^{n} d_{piv,i} - d_{true} \quad (1)$$

$$\varepsilon_{rms} = \sqrt{\frac{1}{n} \sum_{i=1}^{n} (\overline{d_{piv}} - d_{piv,i})^2} \quad (2)$$

where,

d_{piv}– Displacement evaluated by PIV, d_{true}– true displacement measured by LVDT and

$\overline{d_{piv}}$ – The mean displacement evaluated by PIV

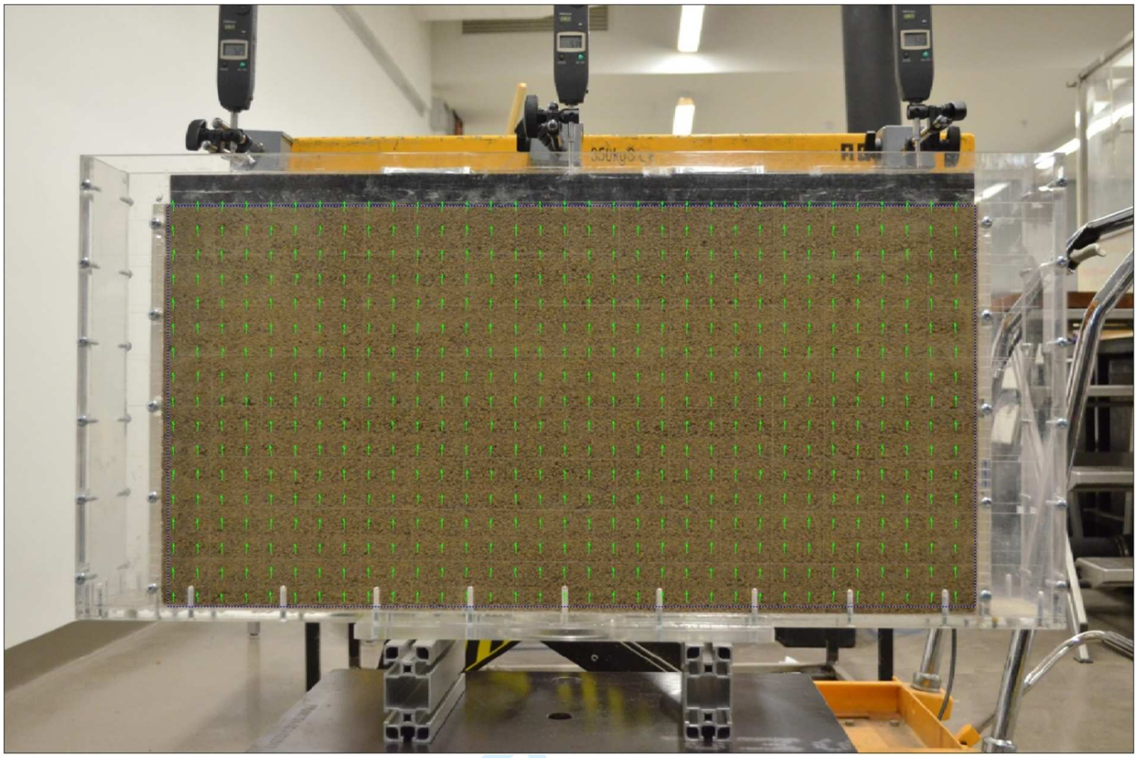

Figure 7 Estimated displacement vectors for 1 mm translation (every 5th vector is shown)

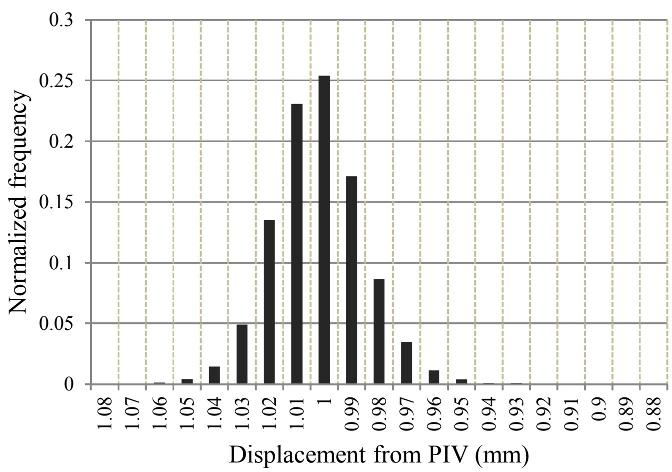

Figure 8 Normalised distribution of estimated displacements in object -space corresponds to 1 mm true displacement

Results and Discussion

Process of cavity initiation and evolution

The important stages of some selected drainage cycles (3, 4 and 12) are shown in Figure 9. Stage 1 is prior to water inflow and Stage 2 is the end of water inflow. Stages 3 and 4 represent the end of water stabilisation (2 minutes from the 2nd step) and the end of water drainage, respectively. In Stages 2 and 3, the capillary force between soil particles is lost as the soil becomes saturated, and this action creates potential loosening areas in the soil model. Then, in Stage 4, the water runs towards the crack as the valve is opened. Therefore, particles near the crack are drained first and this was evident from the very first drainage cycle. When the water is draining the system, the capillary force begins to build up due to the decrease in the degree of saturation. The cavity is only developed during the third cycle when the effective stress in the most loosened zone becomes zero, as shown by the dotted circle in the 3rd stage of Figure 9 (a).

The initial cavity has a shape of a fan, with a slope on both sides and arching over the top, and this is shown by the dotted circle in Figure 9. A similar shape was observed in the laboratory model test conducted by Sato and Kuwano (2010) to investigate the erosion rate when an underground structure is close to a defective pipe. The cavity size becomes greater with the number of cycles. However, the propagation of the cavity towards the model ground is dependent on other factors, such as the height between the existing cavity ceiling and the model base (H_{cc}) before water release and the maximum recorded height of the water level (H_{max}). Table 3 presents the measured H_{cc} and H_{max} corresponding to each drainage cycle. It was clearly noted that for cavity propagation to take place, the volume of subsequent water cycles must be larger than the previous one. It is essential for the water table to rise above the cavity to saturate the soil at the upper extent of the cavity. Table 3 depicts that, whenever the H_{max} exceeds H_{cc}, the existing cavity loses its stability, changes its shape and propagates further upwards. This can be observed in Figure 9 (b) and (c) which show the cavity propagation for the 4th and 12th drainage cycles. During the fourth cycle, water perturbation exceeds the upper extent of the cavity, making the cavity unstable and triggering it to move upwards. Conversely, in cycle number 12, the cavity is stable, because the water level does not exceed the upper extent of the cavity.

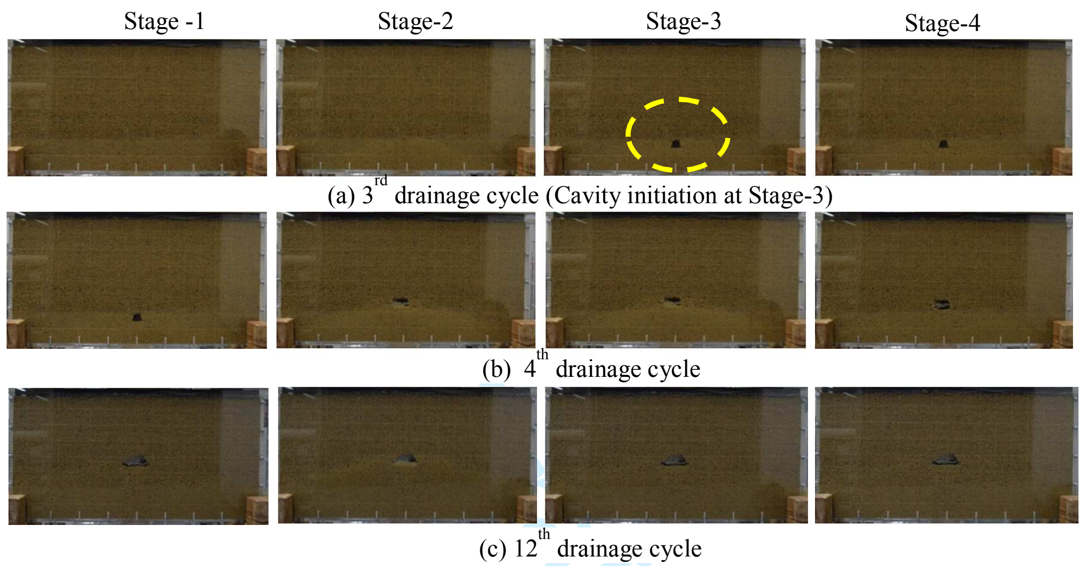

Figure 9: Stages of cavity evolution: (a) 3rd drainage cycle, (b) 4th drainage cycle, (c) 12th drainage cycle

Rate of soil loss and grading of the eroded soil

The individual and accumulated dry weights of the eroded soil corresponding to each drainage cycle are shown in Figure 10. As illustrated in Table 2, the volume of water inflow was increased after every three consecutive cycles. Therefore, an increment in the eroded soil mass can be expected for the 4th, 7th, 10th, 13th, 16th and 19th cycles. However, inspection of Figure 10 indicates that peaks of soil loss were recorded in cycles 3, 5, 7, 8, 12 and 19. A comparison of Table 2 and Figure 10 shows that it is hard to identify a direct relationship between the eroded mass in terms of H_{cc} and H_{max}. However, it seems that H_{max}/H_{cc} is always greater than or equal to one for cycles with the highest eroded mass, with the exception of cycle 12.

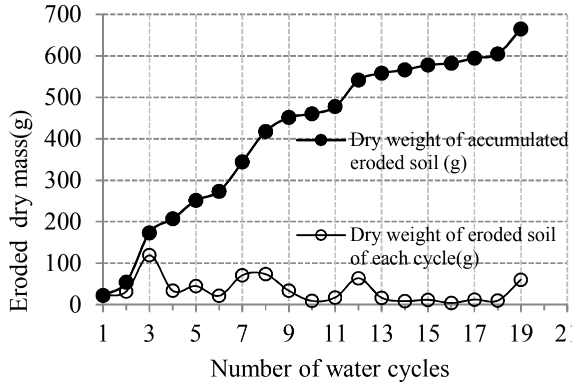

Figure 10: Eroded soil mass in each drainage cycle

The particle size distribution of the eroded dry mass of soil was obtained for each individual cycle. The measured soil mass corresponding to each range of grain size is plotted in Figure 11 against the expected mass, which was calculated based on the original grain size distribution of the material (Figure 5). It is evident from Figure 11 that, compared to the original material, there is a higher percentage of particles which are smaller than 0.3 mm in the eroded mass and this size of particle is highly susceptible to erosion. In comparison the 0.3 to 1.18 mm particle range seems to have higher erosion resistance, while the 1.18 to 4.75 mm range follows the original grain size distribution closely.

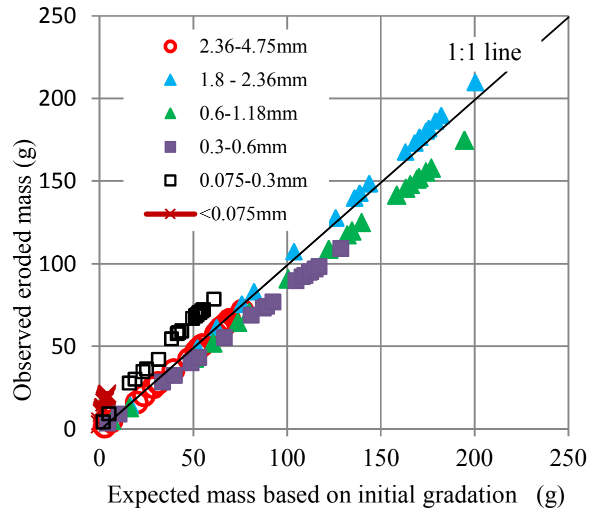

Figure 11: Grain size of eroded mass

Particle movement tracking with PIV

Particle movement tracking corresponding to each stage of the cycle was possible using PIV analysis. Velocity profiles for the 1st and 2nd stages of cycle 4 are presented in Figure 12 as examples. The saturated area close to the water inlet had a monotone colour due to the presence of a greater amount of water and, therefore, deformation in that region is difficult to track using this method. Figure 12 shows that significant particle settlement occurred in the upper layers not only during the drainage period but also during the period of water inflow. The downward arrows refer to the soil particles moving downward from the original position. Therefore, the method permits the identification of the flow path and the area affected by large deformation.

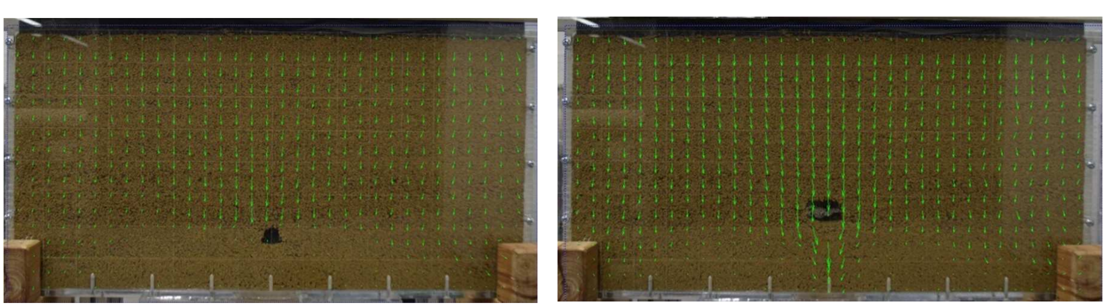

(a) (b)

Figure 12: Velocity profile for 4th cycle: (a) During Stage 2 and 3, (b) During Stage 4

Evaluation of vertical deformation

Using PIVlab, the horizontal and vertical component of the velocity for each test patch was obtained. This method creates a high vector resolution (vectors per unit area) within the image. To simplify the interpretation of the deformation profile in model space, the area-mean velocity of a 50 x 50 mm^2 area in the model space (see Figure 13 (a)) was considered. Only the vertical component of the mean velocity vector of each 50 x 50 mm^2 was calculated and downward movement was considered as settlement. The displacement distribution in model space is plotted in Figure 13 (b) – (d), based on the mean area velocities calculated above.

Inspection of Figure 13 (b) reveals that the settlement for all the layers in the 1st cycle had similar trends in the central region, which is located over the pipe defect. As shown in Figure 12, the initial cavity was formed during the 3rd cycle close to the top edge of the 2nd layer. Therefore, the settlement of the middle part of the 4th layer of the 3rd cycle was increased and deviated from the rest of the layers, as shown in Figure 13 (c). This trend is clearly illustrated in the 4th cycle (Figure 13 (d)) as the cavity was further propagated upwards and the influence on the 4th layer was greater than that on the 3rd cycle. The settlement of the 8th layer was almost uniform, but closer to the left and right boundaries. At these two extreme ends, the highest displacement was always recorded in the 8th layer and the displacement was gradually decreased with the depth. This trend could be due to the boundary effects and differential stress distribution of externally-applied overburden pressure.

To more fully understand the influence of cavity depth on ground surface displacement troughs, the difference in the deformation behaviour close to the cavity and close to the ground surface were considered. Individual and cumulative displacements over the pipe defect at the 4th, 5th, 6th, 7th and 8th layers for all nineteen cycles are plotted in Figure 14. It can be clearly seen in Figure 14 that each time the period of water inflow is increased after three consecutive cycles, the recorded layer displacement increased for those cycles, although comparatively higher settlements were observed during the first five cycles. This may be due to the initial cavity formation, rapid cavity transformation, and propagation during the 3rd to 5th cycles. In addition, for the first few cycles, when the water enters the tank, the degree of saturation is increased in the lower layers and hence, settlement occurs throughout the layers due to the reduction of the pore water pressure which reduces the apparent cohesion of the partially saturated ground. Since the 4th and 5th layers are affected by erosion in the 8th and 13th cycles, layer 4 and 5 were discontinued for the rest of the cycles in the plot cycle.

Ground settlement troughs due to ground arching similar to Figure 13 have been observed in the past using physical and analytical modeling of active trapdoor systems (Terzaghi 1936; Stone and Wood 1992; Ono and Yamada 1993; Santichaianaint 2002; Costa et al. 2009). Most previous studies used trap-door tests in dry granular material or clay where the soil had no opportunity to escape through the trap door. In most cases, soil flows under gravity due to the loss of support and settlement is a function of trap-door width, the distance of trap-door movement and the shear strength of the soil. As in this study, settlement is induced by the water flow and the scale of the settlement is affected by both the hydraulic conditions and the crack width configurations (Rogers 1986; Mukunoki et al. 2009).

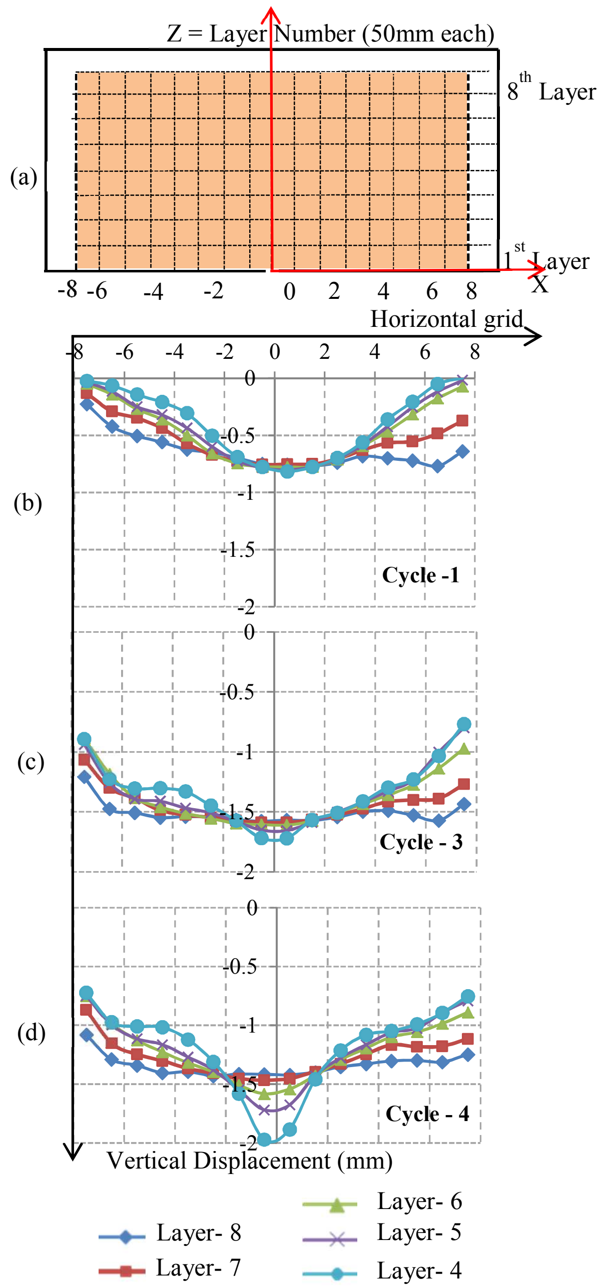

Figure 13: Vertical settlement of the model ground at different layers; (a) Defined grid distribution in model tank; (b) Settlement for cycle 1; (c) Settlement for cycle 3; (d) Settlement for cycle 4

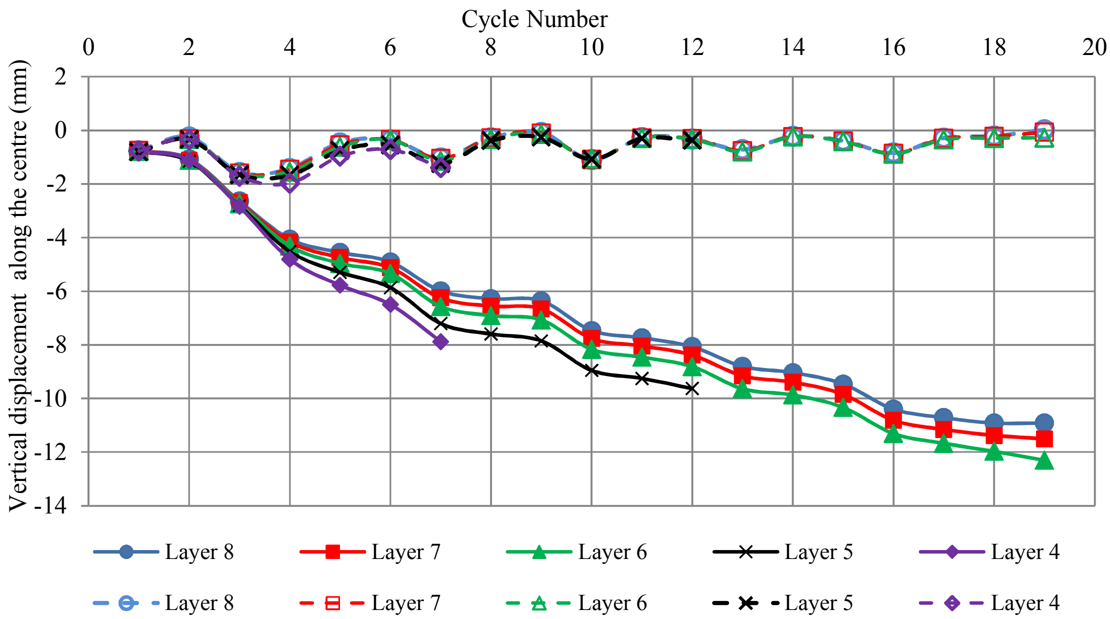

Figure 14: Cumulative and individual settlement of layers along the central vertical line

Summary

Previous research has documented the effects of defective sewer pipes in the development of localised sinkholes and the associated consequences. However, these studies have either been qualitative or focused primarily on the internal stability of the cavity and the ground displacement in the vicinity of the pipe has not been addressed in detail. During the process of sinkhole development/formation, the surrounding ground is always subjected to gradual deformation prior to surface subsidence. Therefore, a reliable method that can describe the effect of pipe defects and associated internal erosion on ground displacement is essential. In this study, an efficient internal erosion test apparatus utilising the PIV technique, is introduced. This technique is capable of directly investigating the eroded soil mass and graduation under consecutive drainage cycles while monitoring the ground displacement at a higher resolution than can be achieved using displacement transducers. Preliminary experiments were performed using a poorly-graded sand which is compatible with a sewer pipe bedding material approved by Australian standards (Standards Australia 2002). Soil loss and the displacement induced by consecutive exfiltration and infiltration through pipe defects were evaluated based on the laboratory model test results. Images were acquired from both sides of the apparatus throughout the experiment and the displacement field was generated based on PIV.

Although the proposed method is convenient and economical, the testing apparatus showed some limitations, particularly due to skin friction in the first few cycles. As explained in the previous section, the friction effect is minimal in this particular experimental set-up. However, complete elimination of the friction effect will improve the test results. The best option to eliminate the friction would be to apply a lubricant between two polyethylene sheets inserted between the side wall and the soil (Fang et al. 2004). However, this approach will affect the images taken for PIV analysis due to reflections of light through multiple objects. The other limitation is that the proposed apparatus is not designed to simulate pipe defects at the invert of the pipes. However, it can be easily modified to study various types of pipe defects.

Conclusions

The results are promising and the following is a summary of the conclusions.

- The measured displacement of subsequent layers resting on the pipe was more or less constant above the pipe defect prior to cavity formation. With the entry of water into the model tank, the soil around the defective pipe was saturated and easily migrated into the pipe through the drainage process due to the loss of effective stress. Therefore, a void was formed after a few cycles and a sudden settlement was observed in the area resting on the cavity roof.

- Vertical settlement troughs of soil parallel to the pipe were observed due to ground arching effects and had a cone-shaped distribution that had the maximum displacement exactly above the pipe defect.
- The soil resting above the water table is partially saturated and the effective stresses are higher due to negative pore pressure. Therefore, the cavity ceiling is capable of spanning by itself unless the pipe defect is severe. However, submerged cavities are not stable since saturation of soil decreases the apparent cohesion, which reduces the effective stress. If the cavity ceiling is located above the water table, the cavity is stable and failure is accompanied by submerging the cavity.
- Post-erosion analysis indicated that particles less than 0.3 mm are highly susceptible to erosion through a 5 mm wide pipe defect.
- The PIV technique was effectively implemented in this study to evaluate the failure mechanism due to soil migration near to and far from a pipe defect. Ground displacement troughs due to arching effects can be evaluated at any place and at any stage of the testing process based on image correlation. As an added advantage, this also allows effective tracking of the seepage and drainage path, which is very beneficial for understanding the impact of seepage and drainage path on cavity progression. The suggested approach provides important information to review the suitability of pipe bedding materials against internal erosion through defective pipes. The method is designed with minimal resources and can be easily implemented for granular soil.

For future work, the relationship between the crack width and the maximum particle size of the backfill will be studied for a number of Australian pipe embedment materials and the susceptibility to erosion will be compared. In addition, an analytical solution which can explain soil erosion-induced cavity development due to water inflow and soil drainage will be proposed. The combination of those results would facilitate the understanding of the suitability of pipe embankment materials against internal erosion-induced problems.

Acknowledgements

The first author would like to acknowledge: the technical support received from Mr. Alec Papanicolaou and Mr. Fejas Xhaferii, the senior technical officers of the Faculty of Science, Engineering and Technology at Swinburne University for erecting the testing apparatus, and Swinburne University of Technology for supporting this research by offering a Swinburne University Postgraduate Research Award (SUPRA).

References

Abraham, D.M., and Wirahadikusumah, R. 1999. Development of prediction models for sewer deterioration. *In* Proceedings of the 8th Conference on the Durability of Building Materials and Components. *Edited by* M. A.Lacasse and D.J. Vanier. NRC Research Press, Vancouver, Canada. pp. 1257 - 1267.

Balkaya, M., Moore, I.D., and Sağlamer, A. 2012. Study of non-uniform bedding due to voids under jointed PVC water distribution pipes. Geotextiles and Geomembranes **34**: 39-50. doi: http://dx.doi.org/10.1016/j.geotexmem.2012.01.003.

Benahmed, N., and Bonelli, S. 2012. Internal erosion of cohesive soils: laboratory parametric study. *In* 6th International Conference on Scour and Erosion. SHF, Paris, France. p. 8

Bertrand-Krajewski, J., Cardoso, M., Ellis, B., Frehmann, T., Giulianelli, M., Gujer, W., Krebs, P., Pliska, J., and Pryl, K. 2006. Towards a better knowledge and management of infiltration and exfiltration in sewer systems: the APUSS project. Water Practice & Technology **1**(01).

Brachman, R.W., Moore, I.D., and Rowe, R.K. 2000. The design of a laboratory facility for evaluating the structural response of small-diameter buried pipes. Canadian Geotechnical Journal **37**(2): 281-295. doi: 10.1139/t99-104.

Brachman, R.W., Moore, I.D., and Rowe, R.K. 2001. The performance of a laboratory facility for evaluating the structural response of small-diameter buried pipes. Canadian Geotechnical Journal **38**(2): 260-275.

British Standards Institution. 1987. BS 8005 : Sewerage : Part 1. London, UK. pp. 7-10.

Burenkova, V.V. 1993. Assessment of suffusion in non-cohessive and graded soils. *In* First international conference "Geo-Filters" *Edited by* Brauns and Heibum and Schelur, Karlsruhe, Germany pp. 357-360.

Burn, S., DeSilva, D., Eiswirth, M., Hunaidi, O., Speers, A., and Thornton, J. 1999. Pipe leakage–future challenges and Solutions. *In* Pipes Conference, Wagga Wagga, NSW, Australia.

Cardoso, A., Prigiobbe, V., Giulianelli, M., Baer, E., Bénédittis, J.D., and Coelho, S.T. 2006. Assessing the impact of infiltration and exfiltration in sewer systems using performance indicators: case studies of the APUSS project. Water Practice and Technology **1**(1).

Chang, D.S., and Zhang, L.M. 2013. Extended internal stability criteria for soils under seepage. Soils and Foundations **53**(4): 569-583. doi: http://dx.doi.org/10.1016/j.sandf.2013.06.008.

Corps of Engineers. 1953. The Unified Soil Classification System, U.S. Army Technical Memorandum. *In* No. 3-357, Vol. 1 (Revised April, 1960)

Costa, Y.D., Zornberg, J.G., Bueno, B.S., and Costa, C.L. 2009. Failure Mechanisms in Sand over a Deep Active Trapdoor. Journal of Geotechnical and Geoenvironmental Engineering **135**(11): 1741-1753. doi: doi:10.1061/(ASCE)GT.1943-5606.0000134.

Davies, J.P., Clarke, B.A., Whiter, J.T., and Cunningham, R.J. 2001. Factors influencing the structural deterioration and collapse of rigid sewer pipes. Urban Water **3**(1–2): 73-89. doi: http://dx.doi.org/10.1016/S1462-0758(01)00017-6.

Drainage Services Department. 2013. Sewerage Manual (Part 1) – Key Planning Issues and Gravity Collection System. Government of the Hong Kong, Special Administrative Region, Hong Kong.

El-Qady, G., Hafez, M., Abdalla, M.A., and Ushijima, K. 2005. Imaging subsurface cavities using geoelectric tomography and ground-penetrating radar. Journal of Cave and Karst Studies **67**(3): 174-181.

Fang, Y., Chen, T., Holtz, R., and Lee, W. 2004. Reduction of Boundary Friction in Model Tests. Geotechnical Testing Journal **27**(01): 1-10. doi: https://doi.org/10.1520/GTJ10812.

Fenner, R.A. 1991. Influence of sewer bedding arrangements on infiltration rates on soil migration. Proceedings of ICE, Municipal Engineer (Institution of Civil Engineers) **8**: 105 - 117.

Galve, J.P., Gutiérrez, F., Guerrero, J., Alonso, J., and Diego, I. 2012. Optimizing the application of geosynthetics to roads in sinkhole-prone areas on the basis of hazard models and cost-benefit analyses. Geotextiles and Geomembranes **34**: 80-92. doi: http://dx.doi.org/10.1016/j.geotexmem.2012.02.010.

Guo, S., Shao, Y., Zhang, T., Zhu, D., and Zhang, Y. 2013. Physical Modeling on Sand Erosion around Defective Sewer Pipes under the Influence of Groundwater. Journal of Hydraulic Engineering **139**(12): 1247-1257. doi: 10.1061/(ASCE)HY.1943-7900.0000785.

Indraratna, B., Dilema, E., and Vafai, F. 1996. An experimental study of the filtration of a lateritic clay slurry by sand filters. Proceedings of the ICE-Geotechnical Engineering **119**(2): 75-83.

Institute of Public Works Engineers Australia. 2010. Specification for Supply of Recycled Material for Pavements, Earthworks and Drainage 2010. Department of Environment, Climate Change and Water, NSW.

Istomina, V.S. 1957. Filtration stability of soils. Gostroizdat, Moscow, Leningrad.

Karpf, C., Hoeft, S., Scheffer, C., Fuchs, L., and Krebs, P. 2011. Groundwater infiltration, surface water inflow and sewerage exfiltration considering hydrodynamic conditions in sewer systems. Water Science and Technology **63**(9): 1841-1848.

Ke, L., and Takahashi, A. 2014. Triaxial erosion test for evaluation of mechanical consequences of internal erosion. Geotechnical testing Journal **37**(March 2014): 347-364.

Kenney, T.C., and Lau, D. 1985. Internal stability of granular filters. Canadian Geotechnical Journal **22**(2): 215-225. doi: 10.1139/t85-029.

Kuwano, R., Hiorii, T., Kohashi, H., and Yamauchi, K. 2006. Defects of Sewer Pipes Causing Cave-ins' in the Road. *In* 5th International Symposium on new technologies for urban safety of mega cities in Asia (USMCA), Phuket, Thailand

Kuwano, R., Kohata, Y., and Sato, M. 2012. A case study of ground cave-in due to large scale subsurface erosion in old land fill. *In* ICSE6, Paris. pp. 265-271.

Liu, J., Liu, M., and Zhu, Z. 2011. Sand Deformation around an Uplift Plate Anchor. Journal of Geotechnical and Geoenvironmental Engineering **138**(6): 728-737. doi: 10.1061/(ASCE)GT.1943-5606.0000633.

Meguid, M.A., and Dang, H.K. 2009. The effect of erosion voids on existing tunnel linings. Tunnelling and Underground Space Technology **24**(3): 278-286. doi: http://dx.doi.org/10.1016/j.tust.2008.09.002.

Moore, I. 2008. Assessment of damage to rigid sewer pipes and erosion voids in the soil, and implications for design of liners. *In* 2008 No-Dig Conference & Exhibition, North American Society for Trenchless Technology, Dallas, Texas.

Mukunoki, T., Kumano, N., and Otani, J. 2012. Image analysis of soil failure on defective underground pipe due to cyclic water supply and drainage using X-ray CT. Frontiers of Structural and Civil Engineering **6**(2): 85-100. doi: 10.1007/s11709-012-0159-5.

Mukunoki, T., Kumano, N., Otani, J., and Kuwano, R. 2009. Visualization of Three Dimensional Failure in Sand due to Water Inflow and Soil Drainage from Defective Underground Pipe Using X-RAY CT. Soils and Foundations **49**(6): 959-968. doi: 10.3208/sandf.49.959.

Mukunoki, T., Otani, J., and Kuwano, R. 2007. Visualization of cavity generation in soils on sewerage defects using X-ray. *In* Proc. Of the 13th Asian Regional Conference on Soil Mechanics and Geotechnical Engineering, Kolkata, India. pp. 485-488.

Mukunoki, T., Otani, J., Nonaka, S., and Horii, T. 2006. Evaluation of cavity generation in soils subjected to sewerage defects using X-ray CT. *In* International Workshop GeoX2006, Aussois, France. pp. 365 -371.

Ng, C.W.W., Zhan, L.T., and Cui, Y.J. 2002. A new simple system for measuring volume changes in unsaturated soils. Canadian Geotechnical Journal **39**(3): 757-764.

O'Reilly, M.P., Rosbrook, R.B., Cox, G.C., and McCloskey, A. 1989. Analysis of defects in 180 km of sewer pipes in Southern water authority. .

Ono, K., and Yamada, M. 1993. Analysis of the arching action in granular mass. Géotechnique **43**(1): 105-120. doi: doi:10.1680/geot.1993.43.1.105.

Otani, J., Mukunoki, T., and Obara, Y. 2000. Application of X-ray CT method for characterisation of failure in soils. Soils and Foundations **40(2)**: 113-120.

Raffel, M., Willert, C.E., Wereley, S.T., and Kompenhans, J. 2007. Particle Image Velocimetry- A Practical Guide. 2 ed. Springer, New York

Renuka, I.H.S. 2012. Evaluation of ground loosening behavior and mechanical properties of loosened sand associated with underground cavities. *In* Department of Civil Engineering. University of Tokyo, Japan, UTokyo Repository , http://hdl.handle.net/2261/52578.

Renuka, I.H.S., and Kuwano, R. 2011. Formation and evaluation of loosened ground above a cavity by laboratory model tests with uniform sand. *In* Proc. 13th International summer symposium, Uji, Kyoto, Japan. pp. 211-214.

Rogers, C.J. 1986. Sewer deterioration studies the background to the structural assessment procedure in the sewerage rehabilitation manual. Water Research Centre.

Santichaianaint, K. 2002. Centrifuge modeling and analysis of active trapdoor in sand. *In* Department of Civil, Environmental and Architectural Engineering,. University of Colorado at Boulder.

Sato, M., and Kuwano, R. 2008. Experimental study on evaluation of loose ground surrounding a cavity in soil. *In* 7th International symposium on new technologies for urban safety of mega cities in Asia, USMCA, Beijing, China. pp. 751-758.

Sato, M., and Kuwano, R. 2010. Model tests for the evaluation of formation and expansion of a cavity in the ground. *In* 7th International Conference on Physical Modelling in Geotechnics Switzerland:. pp. 581-586.

Sato, M., and Kuwano, R. 2013. Effects of buried structures on the formation of underground cavity. *In* 18th International Conference on Soil Mechanics and Geotechnical Engineering, Paris. pp. 1769-1772.

Sato, M., and Kuwano, R. 2015a. Influence of location of subsurface structures on development of underground cavities induced by internal erosion. Soils and Foundations **55**(4): 829-840. doi: http://dx.doi.org/10.1016/j.sandf.2015.06.014.

Sato, M., and Kuwano, R. 2015b. Suffusion and clogging by one-dimensional seepage tests on cohesive soil. Soils and Foundations **55**(6): 1427-1440. doi: http://dx.doi.org/10.1016/j.sandf.2015.10.008.

Standards Australia. 1998. AS 1289 : Methods of testing soils for engineering purposes, Method .5.5.1 : Soil compaction and relative dennsity test. Sydney, Australia.

Standards Australia. 2002. AS 2566: Buried Flexible Pipelines. Sydney, Australia.

Stone, K.J.L., and Wood, D.M. 1992. Effects of Dilatancy and Partical Size Observed in Model Tests on Sand. Soils and Foundations **32**(4): 43-57.

Terzaghi, K. 1936. Stress distribution in dry and saturated sand above a yielding trap door. *In* 1st International Conference on Soil Mechanics and Foundation Engineering. Mass, Cambridge. pp. 35-39.

The Mathworks Inc. 2014. MATLAB Ver. 8.3 Release 2014b, . Natick, Massachusetts, USA

Thielicke, W. 2014. The flapping flight of birds : Analysis and application. *In* Department of Ocean Ecosystems. University of Groningen.

Thielicke, W., and Stamhuis, E. 2014. PIVlab - Towards User-friendly, Affordable and Accurate Digital Partical Image Velocimetry in MATLAB. [accessed 20th August 2015].

Tognon, A.R., Kerry Rowe, R., and Brachman, R.W.I. 1999. Evaluation of side wall friction for a buried pipe testing facility. Geotextiles and Geomembranes **17**(4): 193-212. doi: http://dx.doi.org/10.1016/S0266-1144(99)00004-7.

Tohda, J., and Hachiya, M. 2005. Response and design of buried pipelines subjected to differential ground settlement. Proceedings of 16th International Conference on Soil Mechanics and Geotechnical Engineering: 1659-1662.

Tsutsumi, Y., Sato, M., and Kuwano, R. 2010. Local deformation characteristics of model ground with cavity and loosening. *In* 7th International Conference on Physical Modeling in Geotechnics. Taylor and Francis Group, Zurich, Swisterland. pp. 587-592.

United States Department of the Interior. 1996. Pipe Bedding and Backfilling. *In* Geotechnical Training Manual No.7. Bureau of Reclamation, Technical Service Center, Geotechnical Services, Denver, Colorado

Water Services Association Australia. 2002. Sewerage code of Australia, Melbourne retail water agencies edition, Version 1.0, (WSA 02-2002-2.3). Melbourne, Australia.

Weil, G.J. 1995. Remote infrared thermal sensing of sewer voids. *In* Proceedings of the international Society for Optics and Photonics (SPIE), Oakland, CA. pp. 229-237.

Yarra Valley Water. 2013. Pipe embedment and trench backfill , Power Point Presentation for Asset Creation Learning Forum. Yarra Valley Water, Melbourne.

Zheng, T. 2007. Nonlinear finite element study of deteriorated rigid sewers including the influence of erosion voids. *In* Department of Civil Engineering. Queen's University., Kingston, Ontario, Canada.

Tables

Table 1: Basic engineering properties of Dromana sand

Property	Value
Coefficient of uniformity, C_u	3.93
Coefficient of curvature, C_c	1.016
Maximum particle size, D_{max} (mm)	4.75
Maximum void ratio, e_{max}	0.96
Minimum void ratio, e_{min}	0.59
Specific gravity, G_s	2.52
Fines content, F_c (%)	0.64
Optimum moisture content (%)	11
Maximum (standard proctor) dry density (kg/m^3)	1931

Table 2: Duration and total volume of water inflow

Cycle No	Duration of inflow (s)	Water inflow (ml)
1, 2, 3	30	330
4, 5, 6	60	660
7, 8, 9	90	990

10, 11, 12	120	1320
13, 14, 15	150	1650
16, 17, 18	180	1980
19	210	2310

Table 3: Stability of cavity with respect to maximum water rise

Cycle No	H_{cc} (mm)	H_{max} (mm)	$H_{max} > H_{cc}$	Stability of the existing cavity
1	-	6.0	No	-
2	-	8.3	No	-
3	-	10.9	No	
4	10.3	14.5	Yes	No
5	14.5	17.4	Yes	No
6	16.9	17.8	Yes	No
7	17.6	19.8	Yes	No
8	19.6	19.7	Coincides	Yes
9	19.6	19.7	Coincides	Yes
10	19.4	21.4	Yes	No
11	20.5	20.7	No	Yes
12	20.6	20.7	No	Yes
13	20.4	22.2	Yes	No
14	23.7	21.4	No	Yes
15	23.7	21.4	No	Yes

16	23.9	23.0	No	Yes
17	23.8	23.2	No	Yes
18	23.6	23.1	No	Yes
19	23.7	24.9	Yes	No

H_{cc} = Height between existing cavity ceiling and tank base; H_{max} = Maximum water level

Figure captions

Figure 1. Schematic diagram of proposed testing apparatus: (a) Front view; (b) Side view; (c) Bottom view

Figure 2. Annotated image of actual erosion test apparatus

Figure 3. Soil/Water Drainage Unit

Figure 4. Interchangeable crack width plate

Figure 5. Particle size distribution of Dromana sand

Figure 6. Arrangement of testing equipment

Figure 7. Estimated displacement vectors for 1 mm translation (every 5^{th} vector is shown)

Figure 8. Normalised distribution of estimated displacements in object -space corresponds to 1 mm true displacement

Figure 9. Stages of cavity evolution: (a) 3^{rd} drainage cycle, (b) 4^{th} drainage cycle, (c) 12^{th} drainage cycle

Figure 10. Eroded soil mass in each drainage cycle

Figure 11. Grain size of eroded mass

Figure 12. Velocity profile for 4th drainage cycle: (a) During stage 2 and 3, (b) During stage 4

Figure 13. Vertical settlement of model ground at different layers; (a) Defined grid distribution in model tank; (b) Settlement for cycle 1; (c) Settlement for cycle 3; (d) Settlement for cycle 4

Figure 14. Cumulative and individual settlement of layers along the central vertical line